DETECTION LIMITS IN PHOTOTHERMAL MICROSCOPY

Alexander Gaiduk, Paul V. Ruijgrok, Mustafa Yorulmaz, Michel Orrit

Institute of Physics, Leiden University, P.O. Box 9504, 2300 RA Leiden, The Netherlands

SUPPLEMENTARY INFORMATION

Contents:

A: Thermal and optical constants for selected materials. Photothermal strength for different media

Table A1: Thermal and optical constants for selected materials at room temperature and normal pressure.[1]

media	n	$\left\|\frac{\partial n}{\partial T}\right\|$ [K^{-1}]	C_p [$Jm^{-3}K^{-1}$]	κ [$Wm^{-1}K^{-1}$]	$\Sigma_{PT} = n\left\|\frac{\partial n}{\partial T}\right\|\frac{1}{C_p}$ [$m^3\,J^{-1}$]	$FOM = n\left\|\frac{\partial n}{\partial T}\right\|\frac{1}{\kappa}$ [$m\,W^{-1}$]	$r=\left(\frac{n_{BK7}-n}{n_{BK7}+n}\right)^2$
BK7 glass	1.52	$1.25\cdot10^{-5}$	$2.15\cdot10^{6}$	1.05	$\mathbf{8.84\cdot10^{-12}}$	$1.81\cdot10^{-5}$	**0**
PMMA	1.49	$1.2\cdot10^{-4}$	$1.4\cdot10^{6}$	0.2	$\mathbf{1.28\cdot10^{-10}}$	$8.94\cdot10^{-4}$	$\mathbf{10^{-4}}$
Water	1.33	$9\cdot10^{-5}$	$4.2\cdot10^{6}$	0.56	$\mathbf{2.85\cdot10^{-11}}$	$2.14\cdot10^{-4}$	$\mathbf{4.4\cdot10^{-3}}$
Glycerol	1.473	$2.7\cdot10^{-4}$	$2.6\cdot10^{6}$	0.28	$\mathbf{1.53\cdot10^{-10}}$	$1.42\cdot10^{-3}$	$\mathbf{2.5\cdot10^{-4}}$
Ethanol	1.36	$4.4\cdot10^{-4}$	$1.93\cdot10^{6}$	0.171	$\mathbf{3.11\cdot10^{-10}}$	$3.5\cdot10^{-3}$	$\mathbf{3.1\cdot10^{-3}}$
Hexane	1.37	$5.5\cdot10^{-4}$	$1.5\cdot10^{6}$	0.124	$\mathbf{5.02\cdot10^{-10}}$	$6.08\cdot10^{-3}$	$\mathbf{2.7\cdot10^{-3}}$
Decane	1.413	$6.06\cdot10^{-4}$	$1.61\cdot10^{6}$	0.147	$\mathbf{5.32\cdot10^{-10}}$	$5.83\cdot10^{-3}$	$\mathbf{1.3\cdot10^{-3}}$
Pentane	1.358	$5.99\cdot10^{-4}$	$1.45\cdot10^{6}$	0.136	$\mathbf{5.61\cdot10^{-10}}$	$5.98\cdot10^{-3}$	$\mathbf{3.2\cdot10^{-3}}$
Chloroform	1.45	$6.19\cdot10^{-4}$	$1.434\cdot10^{6}$	0.129	$\mathbf{6.26\cdot10^{-10}}$	$6.96\cdot10^{-3}$	$\mathbf{5.5\cdot10^{-4}}$
Carbon tetrachloride	1.465	$6.12\cdot10^{-4}$	$1.26\cdot10^{6}$	0.104	$\mathbf{7.11\cdot10^{-10}}$	$8.62\cdot10^{-3}$	$\mathbf{3.4\cdot10^{-4}}$
Carbon disulfide	1.63	$8.13\cdot10^{-4}$	$1.25\cdot10^{6}$	0.161	$\mathbf{1.06\cdot10^{-9}}$	$8.23\cdot10^{-3}$	$\mathbf{1.2\cdot10^{-3}}$

[1]Values are from:
(a) Bialkowski, S.E., Photothermal Spectroscopy Methods for Chemical Analysis, Wiley, **1996.**
(b) CRC Handbook of Chemistry and Physics

$$n\left|\frac{\partial n}{\partial T}\right|\left(\frac{1}{C_p}\right)_T$$

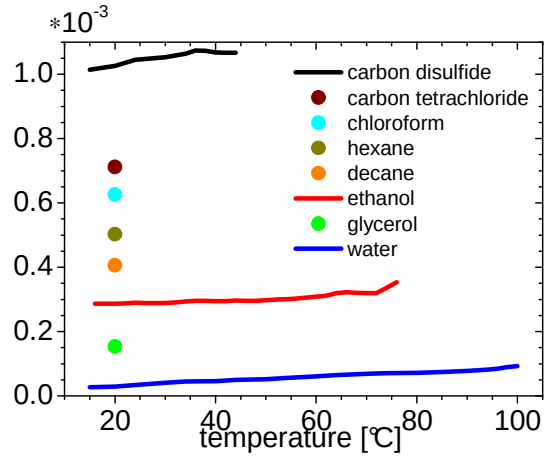

Figure A1: Photothermal strength (Σ_{PT}) for various media. The temperature dependence (as defined by the refractive index behavior with temperature) is shown for water, ethanol and carbon disulfide.

B: Calculated absorption cross-sections for gold nanoparticles of 20 nm and 5 nm in diameter for different wavelengths in media with various refractive indices

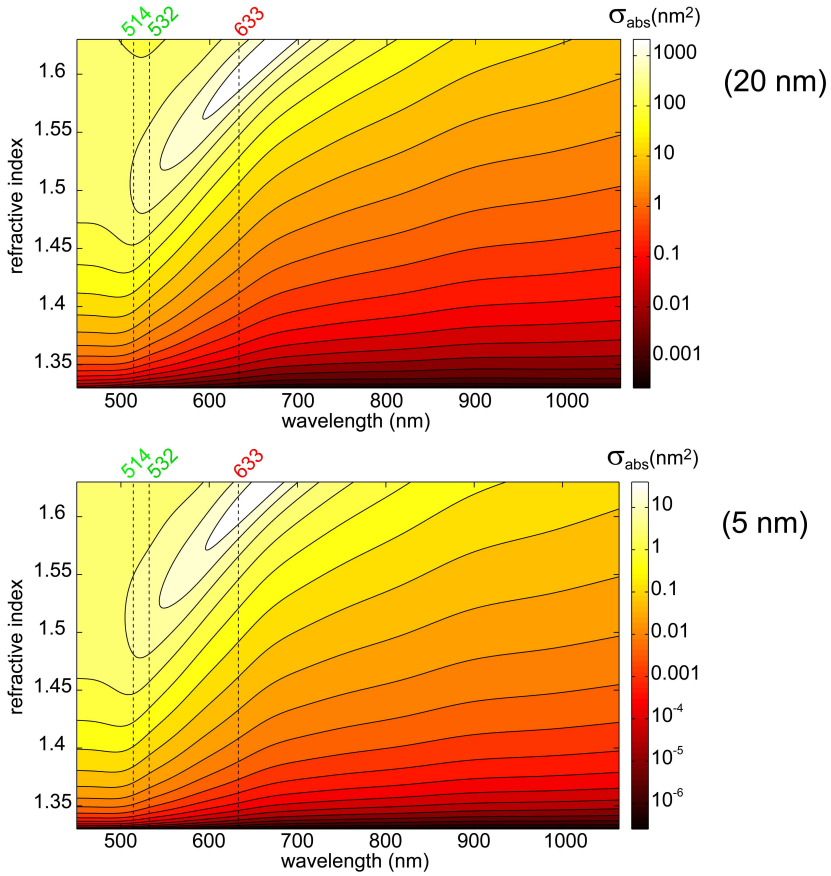

Figure B1: Absorption cross-sections for gold nanoparticles 20 nm and 5 nm in diameter calculated for media with different refractive indices and various wavelengths. Calculations are based on Mie theory [C.F. Bohren, D.R.Huffman 'Absorption and Scattering of Light by Small Particles' Wiley, 1998] and use the dielectric functions of Johnson and Christy [P.B.Johnson, R.W.Christy, 'Optical Constants of Noble Metals' Phys.Rev.B 6 (12) 4370-4379 (1972)]

Table B1: Calculated σ_{abs} (in nm²) for 20 nm diameter gold nanoparticles for selected wavelengths and media.

λ (nm)	refractive index (n)			
	1.63 (carbon disulfide)	**1.47 (glycerol)**	**1.37 (hexane)**	**1.33 (water)**
514	176	463	414	385
532	170	627	453	386.5
633	656	27.1	18.8	16.3
800	104	3.78	2.89	2.59
1064	0.0054	0.77	0.026	0.0003

C: Analysis of the variations of *SNR*

As follows from Eq.4 in the main text, *SNR* is equal to:

$$SNR \approx \frac{1}{\pi\omega_{0.probe}\lambda_{probe}^2\Omega} n\frac{\partial n}{\partial T}\frac{1}{C_p}\frac{\sigma_{abs}}{A}P_{heat}\sqrt{\frac{P_{probe}\Delta t}{h\nu}} \qquad \text{(C1)}$$

where

$\omega_{0.probe}$ is the focal radius (beam waist) of the probe beam
λ_{probe} is the wavelength of the probe light
Ω is the modulation frequency
n is the refractive index of the medium
$\partial n/\partial T$ is the variation of the refractive index of the medium with temperature
C_p is the specific heat capacity of the medium
A is the area of the heating beam in the focal plane ($=\pi\omega_{0.heat}^2$)
P_{heat} is the heating power
P_{probe} is the probe power
$h\nu$ is the energy of the probe photon ($= hc/\lambda_{probe}$)
Δt is the integration time of photothermal detection

Let us consider the equation for the characteristic length of heat diffusion (r_{th}):

$$r_{th}^2 = \frac{2D_{th}}{\Omega} = \frac{2\kappa}{C_p\Omega}, \qquad \text{(C2)}$$

where D_{th} is the thermal diffusivity coefficient, κ is the thermal conductivity of the medium.

Substituting Eq. C2 into C1, we obtain:

$$SNR \approx \frac{1}{\pi\omega_{0.probe}}\left(\frac{r_{th}}{\lambda_{probe}}\right)^2 n\frac{\partial n}{\partial T}\frac{1}{\kappa}\frac{\sigma_{abs}}{A}P_{heat}\sqrt{\frac{P_{probe}\Delta t}{h\nu}} = \frac{1}{\pi\omega_{0.probe}}\left(\frac{r_{th}}{\lambda_{probe}}\right)^2 FOM\,\frac{\sigma_{abs}}{A}P_{diss}\sqrt{\frac{P_{probe}\Delta t}{h\nu}}, \qquad \text{(C3)}$$

where $FOM = n\frac{\partial n}{\partial T}\frac{1}{\kappa}$ is defined as a figure of merit of photothermal media.

Eq. C3 expresses the *SNR* as a function of (i) a combination of thermal and optical parameters of the media $\left(\frac{r_{th}}{\lambda_{probe}}\right)^2 n\frac{\partial n}{\partial T}\frac{1}{\kappa}$ at a given probe wavelength; and (ii) heat and probe power dependent parameters.

In practice, the proportionality parameter in the *SNR* equation, $\left(\frac{r_{th}}{\lambda_{probe}}\right)^2$, is kept close to 1 by choosing the modulation frequency of the heat beam such that r_{th} matches the probe beam waist. Efficient scattering of the probe beam would be achieved in this case.

D: Noise of the photothermal detection

The total noise σ_{total} in the optical experiments, contributed by the detector noise $\sigma_{detector}$, the photon noise σ_{shot} and the laser noise σ_{laser} is defined as follows:

$$\sigma_{total} = \sqrt{\sigma_{detector}^2 + \sigma_{shot}^2 + \sigma_{laser}^2} = \sqrt{\sigma_{detector}^2 + F\sigma_{photon}^2 + \sigma_{laser}^2} = \sqrt{\sigma_{detector}^2 + F\,2BPh\nu + \left(n_{laser}P\right)^2} \qquad \text{(D1)}$$

where $\sigma_{detector}$ is the detector noise, provided by manufacturer, independent of detected power
F is excess noise factor, resulting from the excess noise generated by the photodiode
B is the measurements bandwidth
P is the measured power
$h\nu$ is the energy of the detected photons
n_{laser} is the proportionality coefficient describing the laser noise dependent on the laser power

The noise measured for the Ti:sapphire laser (Mira, Coherent, pumped with Coherent Verdi V10) and the photodetector at different gains is depicted in Fig. D1. There is no contribution of the noise that scales linearly with the laser power within the range of powers we measured, from 1 μW to 1.8 mW. That suggests a photon-noise limited detection of the photothermal signal.

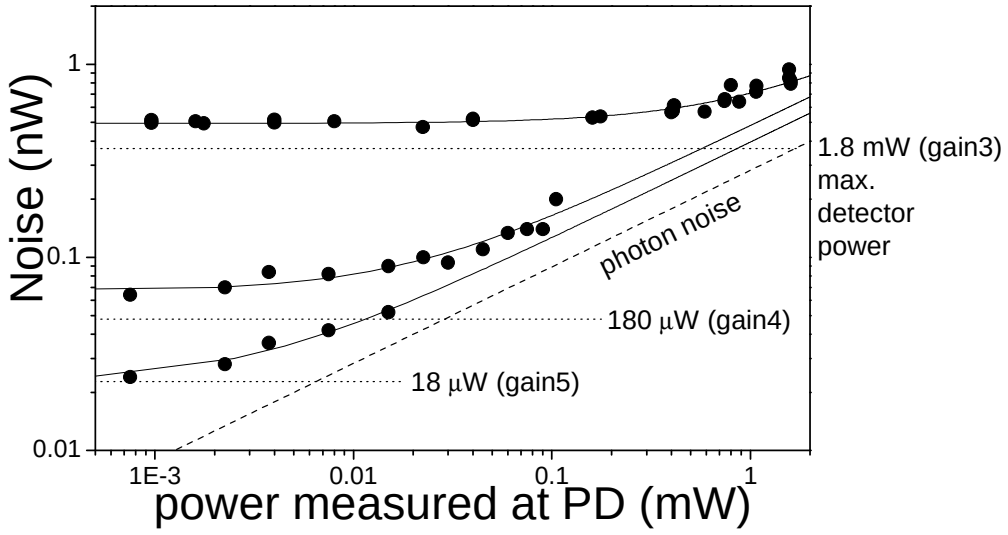

Figure D1. Noise power as a function of the optical power measured at the photodetector (PD). Horizontal dotted lines indicate the detector noise at a given sensitivity (detector gain). These lines also indicate the maximum detector power at a given sensitivity as specified by the manufacturer: 180 nW for the gain 10^7 A/V (not pictured), 1.8 μW for the gain 10^6 A/V (not pictured), 18 μW for the gain 10^5 A/V, 180 μW for the gain 10^4 A/V, 1.8 mW for the gain 10^3 A/V and 18 mW for the gain 10^2 A/V (not pictured). The sensitivity of the Si-PIN detector is specified to be 0.5 A/W in the 770-800nm range. The dashed line represents the calculated photon noise, which scales with the square root of the measured probe power. The results of the noise measurements (for detector gains 10^3-10^5 A/V) are pictured with full dots. Solid lines show results of the fit to the equation below with $\sigma_{detector}$ = 0.49 nW, n_{laser} = 0, F = 3.3 (for 10^3 A/V gain); $\sigma_{detector}$ = 0.067 nW, n_{laser} = 0, F = 2.9 (for 10^4 A/V gain); $\sigma_{detector}$ = 0.023 nW, n_{laser} = 0, F = 2 (for 10^5 A/V gain).

E: Comparison of the "Cat's eye" and "50/50 BS" configurations

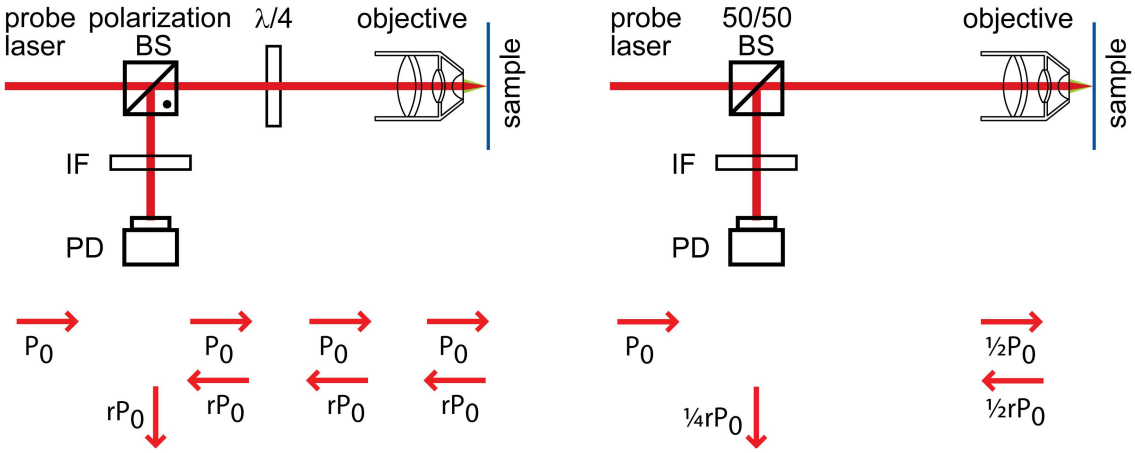

Figure E1. Schematic representation of experimental setup "Cat's eye" (left) and "50/50 BS" (right) configurations and indications of the probe power.

Considering only the effect of probe laser on the photothermal *SNR* for two different reflector configurations we note:

1. For the *"cat's eye"* configuration $S \sim rP_0$, and $N \sim \sqrt{rP_0}$, there r is the reflection coefficient specific to the refraction index contrast at the glass/sample interface. Thus for the "cat's eye" configuration $SNR = \sqrt{rP_0}$.

2. For the *"50/50 BS"* configuration $S \sim \frac{1}{4} rP_0$, and $N \sim \sqrt{\frac{1}{4} rP_0}$, thus $SNR = \frac{1}{2}\sqrt{rP_0}$

The *SNR* should be twice better in the cat's eye configuration, but is experimentally found to be similar to that in the *"50/50 BS"* configuration.

F: AFM measurements of 20 nm gold on glass surface

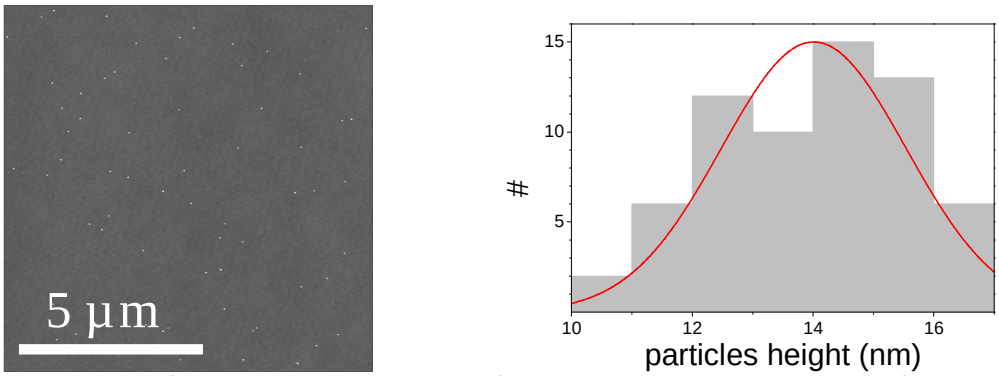

Figure F1. (left) AFM topography image of 20 nm gold particles on glass surface. (right) Histogram of height distributions of these particles (64 particles in total). Mean height is 14±1.5 nm.

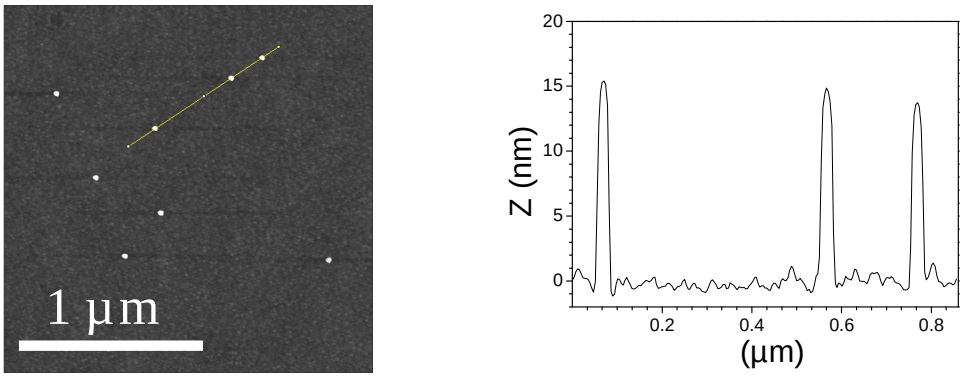

Figure F2. (left) AFM topography image of 20 nm gold particles on glass surface (zoom in to the area of the image presented in G1). (right) A cross section along the line indicated in the image shows the height for three particles.

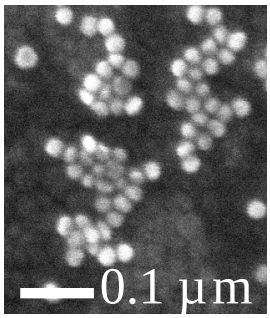

Figure F3. SEM image of 20 nm gold particles

G: Analysis of the PMMA layer thickness

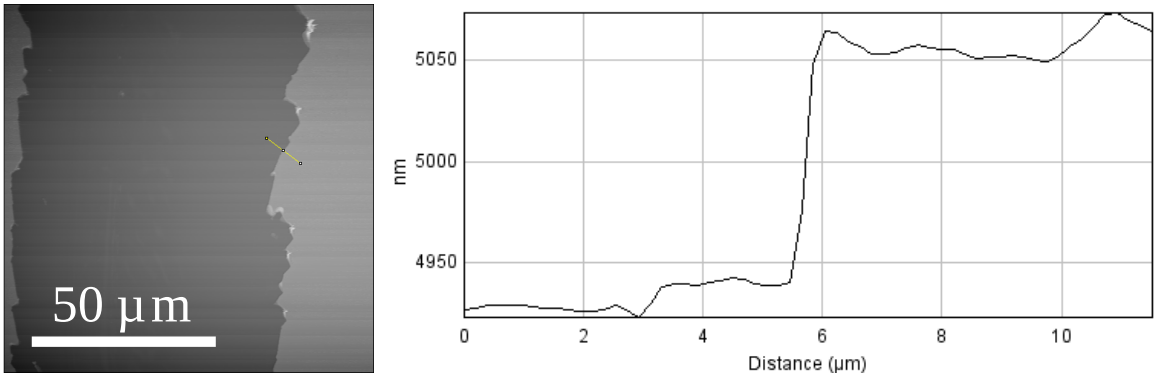

Figure G1: (Right): AFM topography image of a scratch on the PMMA film. The PMMA layer is prepared by spin coating 50 µL of 30 g/L PMMA solution in toluene. (Left): A cross section at the position indicated in AFM image. The height of the PMMA layer is about 100 nm.

H: Analysis of the number of dye molecules in fluorospheres

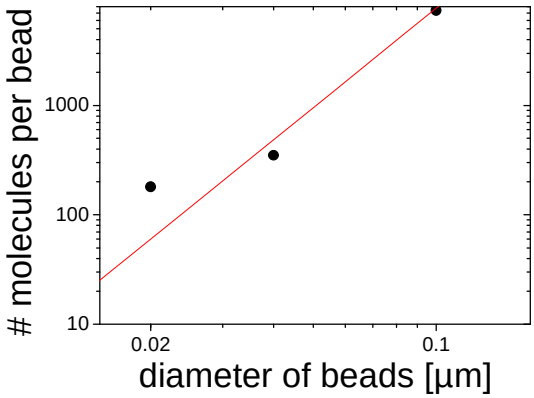

Figure H1: Number of dye molecules per fluorescent bead of various diameters as suggested by Invitrogen manual "FluoSpheres® Fluorescent Microspheres" [http://probes.invitrogen.com/media/pis/mp05000.pdf] for yellow-green beads (fluorescein doping). In our experiment, we used Nile Red beads, which have a different number of dyes per bead.

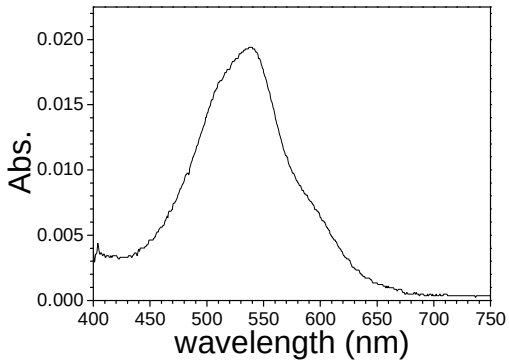

Figure H2: Absorption spectrum of Nile red beads in water solution measured with a SHIMADZU Spectrophotometer UV170 PharmaSpec. On average, assuming all the dye molecules are embedded in the beads, the number of dye molecules per fluorescent bead estimated from the extinction coefficient would be about 30. However, free dye molecules present in solution may contribute to the absorption spectrum and would reduce the actual number of dyes per single bead. The molar extinction coefficient $\varepsilon = 38000\ M^{-1}cm^{-1}$ at 519.4 nm.
[http://omlc.ogi.edu/spectra/PhotochemCAD/html/nilered.html and M. M. Davis and H. B. Hetzer, "Titrimetric and equilibrium studies using indicators related to Nile Blue A," Anal. Chem., 38, 451-461, 1966]

Calculations of the number of dye molecules per single bead:

1. 20 nm Nile Red beads are 2 wt% in the stock solution. Volume of a bead is $4 \cdot 10^{-21}$ L and there are $c_{bead.stock} = 5 \cdot 10^{18}$ beads/L
2. stock solution is diluted in water with 1:100 ratio, resulting in $c_0 = c_{bead.stock}/100 = 5 \cdot 10^{16}$ beads/L
3. the extinction of the sample with c_0 beads concentration is 0.017 - 0.024 = εcL (see Fig.H2). $\varepsilon = 38000\ M^{-1}cm^{-1}$, L=0.2 cm.
4. Estimate of dye molecule concentration: $c = 2.24 \cdot 10^{-6}$ - $3.2 \cdot 10^{-6}$ M/L, thus of molecules $n = c\ N_A = 1.35 \cdot 10^{18}$ - $1.93 \cdot 10^{18}$ molecules/L
5. thus the number of dye molecules per bead is $N = n/c_0$ = 27-39 molecules/bead

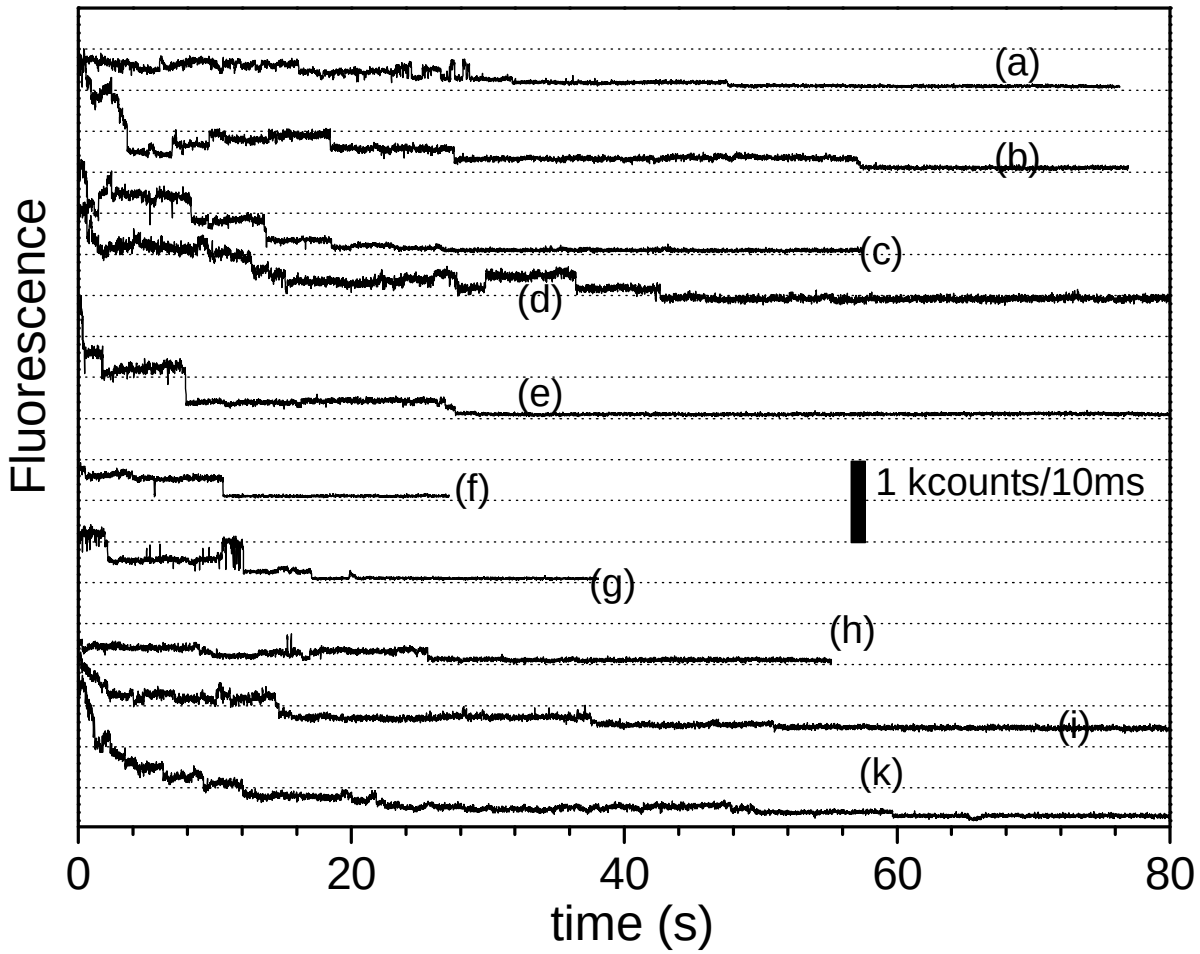

Figure H3: Examples of fluorescence bleaching time traces taken on several 20 nm beads. Traces show single step photobleaching and blinking events, indicating that only few dye molecules are embedded in each bead. Assuming the count rate per single molecule of 100 counts/10 ms (from a single-step photobleaching event with the smallest signal difference with dark counts), a single bead would contain N=2000/100=20 fluorescent dyes. This number corresponds well to the number of dyes estimated from the absorption measurements (Fig.H2), but disagrees with the number provided by the manufacturer for another dye (Fig.H1). Excitation power in the experiment: $P_{heat} = 4.25\ \mu W$.